Journal of Colloid and Interface Science 554 (2019) 692–704

Contents lists available at ScienceDirect

Journal of Colloid and Interface Science

journal homepage: www.elsevier.com/locate/jcis

Regular Article

Adsorption behavior of arsenicals on MIL-101(Fe): The role of arsenic chemical structures

Zongchen Li [a], Xuemin Liu [a], Wei Jin [b], Qingsong Hu [a], Yaping Zhao [a,*]

[a] School of Ecology and Environmental Science, Shanghai Key Laboratory for Urban Ecological Process and Eco-Restoration in East China Normal University, and Institute of Eco-Chongming, Shanghai 200062, China
[b] School of Environmental Science and Engineering, Tongji University, Shanghai, China

GRAPHICAL ABSTRACT

The chemical structures of arsenic species significantly affect their adsorption behaviors onto MIL-101(Fe) due to the complex adsorption mechanisms including Fe—O—As coordination, hydrogen bonding and π-π stacking interaction.

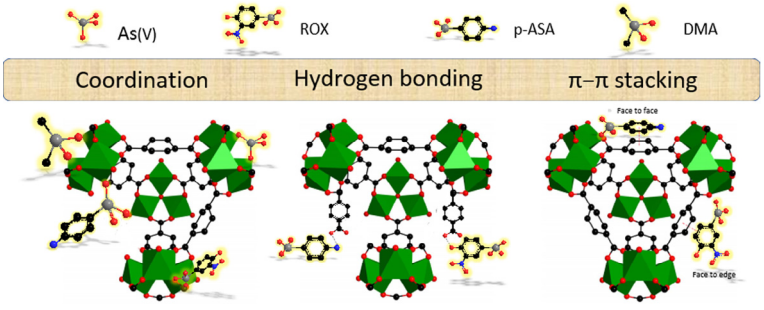

ARTICLE INFO

Article history:
Received 9 May 2019
Revised 6 July 2019
Accepted 16 July 2019
Available online 17 July 2019

Keywords:
Arsenic species
MIL-101(Fe)
Adsorption
Interaction mechanism

ABSTRACT

Arsenic species are regarded as typical water pollutants due to their toxicity. The chemical structures of arsenic species greatly influence their migration and transformation in the environment. Metal-organic frameworks (MOFs) are used as reliable adsorbents to control arsenic contamination, so it is urgently needed to study the effect of chemical structure of arsenic species during adsorption process. The adsorption behaviors of arsenate (As(V)) and its organic forms such as roxarsone (ROX), p-arsanilic acid (p-ASA) and dimethyl arsenate (DMA) by MIL-101(Fe), a type of highly porosity iron-based MOFs in aqueous environment were detailed investigated. The adsorption kinetics of those arsenic species on MIL-101(Fe) is rapid followed with pseudo-second-order kinetic model. MIL-101(Fe) exhibits excellent adsorption capacities for As(V), ROX, p-ASA and DMA with maximum adsorption capacities of 232.98, 507.97, 379.65 and 158.94 mg g^{-1}, respectively. The formed Fe—O—As inner-sphere coordination between arsenic species and the incomplete-coordinated cationic Fe in the MIL-101(Fe) cluster is the primary adsorption mechanism based on FTIR and XPS analysis. Substituent aromatic units in ROX and p-ASA strengthen the adsorption on MIL-101(Fe) through hydrogen bonds and π-π stacking interaction, resulting in higher adsorption capacities far beyond that of As(V) and DMA. The reusability of MIL-101(Fe) is limited by the strong Fe—O—As coordination. These results confirm MIL-101(Fe) a reliable adsorbent to control the aqueous arsenic species contamination and emphasize the significant role of the chemical structure of arsenic speciation on adsorption performances of MOFs.

* Corresponding author.
E-mail address: ypzhao@des.ecnu.edu.cn (Y. Zhao).

https://doi.org/10.1016/j.jcis.2019.07.046
0021-9797/

1. Introduction

Arsenic, a ubiquitous element in the environment, originates from geological processes and anthropogenic activities. Arsenic exists predominantly in inorganic forms such as arsenite (As(III)) and arsenate (As(V)) as well as organic forms such as methylated or aromatic organoarsenicals. Methylated organoarsenicals such as monomethylarsenic acid (MMA), dimethylarsenic acid (DMA) are extensively used as herbicides and pesticides [1]. Aromatic organoarsenicals such as p-arsanilic acid (p-ASA) and roxarsone (ROX) are also widely used as feed additives in livestock and poultry industry due to their high performance to control intestinal parasites and prevent dysentery [2,3]. Although organic arsenics are originally low-toxicity [4]. After entering the environment, water-soluble organoarsenicals can be transformed into inorganic arsenite (As(III)) or arsenate (As(V)) by biotical degradation, which would be more toxic to ecosystem [5]. In previous study, elevated levels of the arsenic concentration in drinking water detected in certain countries such as the United States, India, and China had exceeded 10 $\mu g\ L^{-1}$ [6], compared with that of World Health Organization standard [7]. More important, long-term exposure to arsenic-contaminated water would threaten human's health, leading to cancers, arsenicosis and endocrine disorders [8,9]. To minimize the threats, it is necessary to reduce inorganic and organic arsenic compounds from the aqueous or soil environment. Various of strategies have been reported to control inorganic arsenic contamination [10,11], but the methods that can simultaneously remove organoarsenicals are restricted to advanced oxidation [12], photocatalysis [13] and adsorption. Among them, adsorption is regarded as the most promising technique due to its advantages of simple operation, low cost, high efficiency and reusability. Variety of adsorbents have been studied for arsenic removal, including manganese dioxide [14], activated carbon [15], biochar [16], titanium dioxide [17], carbon nanotubes [18] and chitosan [19]. However, some problems still exist in above adsorbents such as low adsorption capacity and selectivity.

Metal-organic frameworks (MOFs), a novel class of porous adsorbents assembled by metal clusters and organic linkers, have attracted substantial research attention in recent years due to their simple synthesis, unique porous structure and diverse compositions. One of the biggest advantages of MOFs is their inherent coordinatively unsaturated sites (CUSs), i.e. the Lewis acid sites in the structure of MOFs which make them better to interact with guest molecules and reaction intermediates, resulting in the potential application in catalysis and adsorption [20–22]. Intensive studies have been carried out to exploit the potential application of MOFs for arsenic removal, which found that MOFs presenting reliable adsorption affinity and capacity for arsenic are mainly Fe-based MOFs or Zr-based MOFs due to the strong M—O—As (M means metal clusters in MOFs) coordination between metal clusters and arsenic [23–31]. Although the adsorption of arsenicals on MOFs has been studied widely, previous researches only conducted with single type (inorganic or organic) of arsenic and MOFs. The chemical structures of arsenic species greatly influence their adsorption behaviors on variety adsorbents. For instance, Our previous studies focused on the adsorption behaviors of different arsenic species onto $MnFe_2O_4$ magnetic nanoparticles revealed that the adsorption capacity in the order of As(V) > ROX ≈ p-ASA > DMA because the formation of Fe—O—As coordination is the unique adsorption mechanism [32]. Meanwhile, α-FeOOH@GCA showed adsorption capacity in the order of p-ASA > As(V) > DMA due to the extra adsorption interaction for organoarsenicals with graphene oxide [33]. It is noteworthy that the adsorption mechanism of organoarsenicals onto MOFs is more complex in comparison with inorganic arsenate due to the presence of organic groups in both the structure of MOFs material and organoarsenicals, it may result in different adsorption behavior. In order to better apply MOFs for arsenic removal, systematic investigation about the interactions between MOFs and different arsenic species should be highly desired.

Fe-based MOFs are particularly selected in this study because Fe has advantage of environmentally friendly and is one of the most abundant metals in earth's crust. The great adsorption performance of Fe-based MOFs, including MIL-100(Fe), MIL-88A(Fe) and MIL-88B(Fe), on inorganic arsenic have been proven [29,34,35]. However, studies about removal of organoarsenicals are particularly rare [24]. MIL-101(Fe) (MIL stands for Matériaux Institute Lavoisier), a typical Fe-based MOFs, is comprised of octahedral chains of Fe(III) as secondary building units (SBUs) and 1,4-benzenedicarboxylic acid (BDC) linkers [36]. Comparing with other M-BDC polymorphs MIL-53 and MIL-88, MIL-101 shows great potential in adsorption due to relatively high specific surface area and inherent mesoporous cages [37]. Moreover, previous study revealed that MIL-101(Fe) showed great adsorption capacity (up to 107.70 $mg\ g^{-1}$) for phosphate adsorption with reliable recyclability [38]. Considering the same main group of arsenic and phosphor, we expect MIL-101(Fe) to be a potential and suitable adsorbent for arsenic removal.

The aim of this study is to comprehensively understand the effect of chemical structure of arsenic species on adsorption performances by MIL-101(Fe). Inorganic arsenate (As(V)), as well as organoarsenicals including ROX, p-ASA and DMA were selected as representative arsenic species. The adsorption behaviors of these four types of arsenic species onto MIL-101(Fe) have been compared completely, including adsorption kinetics, adsorption isothermals, as well as the effects of pH, competing ions and dissolved organic matters (DOM). Moreover, the possible adsorption mechanisms between arsenic species with different substituent groups and MIL-101(Fe) have been proposed via Fourier transform infrared spectrophotometer (FTIR) and X-ray photoelectron spectroscopy (XPS). Finally, various elution reagents were used to explore the potential reusability of MIL-101(Fe).

2. Materials and methods

2.1. Materials

Aqueous stock solutions of arsenic species (1000 mg-As L^{-1}) were prepared by dissolving disodium hydrogen arsenate heptahydrate ($Na_2HAsO_4{\cdot}7H_2O$, Shanghai Chemical Reagent Institute, 98%), p-arsanilic acid (Aladdin, 98%), roxarsone (Alfa Aesar, 99%) and sodium dimethylarsinate (Alfa Aesar, 98.5%) in deionized water. Arsenic species working solutions of various concentrations (10–400 $mg\ L^{-1}$) were prepared by diluting the stock solutions with deionized water. Ferric chloride hexahydrate ($FeCl_3{\cdot}6H_2O$), terephthalic acid (BDC), *N, N*-dimethylformamide (DMF) and all other chemicals were supplied by Sino pharm Chemical Reagent Co. Ltd (Shanghai, china) and used without further purification.

2.2. Synthesis of MIL-101(Fe)

The MIF-101(Fe) were prepared according to previously reports employing solvothermal method [39]. 2.48 mmol (0.412 g) BDC, 4.9 mmol (1.3244 g) $FeCl_3{\cdot}6H_2O$ were dissolved in 30 mL DMF by sonication. The solution was then transferred to Teflon-lined stainless-steel autoclaves and heated at 110 °C for 20 h. When the autoclaves were cooled down to room temperature, the MIL-101(Fe) powder were respectively washed with DMF and hot ethanol for 3 times to remove unreacted compounds and then dried at 60 °C for 24 h. Before adsorption experiments, the adsor-

bents were activated at 120 °C for 12 h in vacuum dryer to remove moisture.

2.3. Characterization

X-ray diffraction (XRD, Rigaku D/Max-2500, Japan) was carried out to characterize the crystal structure of MIL-101(Fe) with Cu Kα as source of radiation, λ = 1.54056 Å at a scan speed of 10° min^{-1} over the 2θ range from 5° to 80°. Scanning electron microscopy (SEM, JEOL S-4800, Hitachi, Japan) was used to characterize the morphology and particle size of MIL-101(Fe). The BET specific surface area, pore volume and pore size were obtained by nitrogen adsorption-desorption isotherms at 77 K on a Quantachrome Instruments System (02108-KR-1, Quantachrome, USA). Thermogravimetric analysis (TGA) was performed on a STA449 F5 TG-DSC thermal analyzer (Netzsch, Germany) by heating the sample from room temperature to 800 °C with rate of 10 °C min^{-1} under air atmosphere, samples were degassed in vacuum at 120 °C for 24 h before measurements. In situ FTIR (Finnigan Nicolet Nexus 600, Thermo, USA) spectra of MIL-101(Fe) nanoparticles before and after adsorption were collected using the KBr method operated in the scan range of 400–4000 cm^{-1} in transmission mode. X-ray photoelectron spectroscopy (XPS) was carried out to analyze the surface elements of materials on Axis UltraDLD spectrometer (Kratos Analytical-A Shimadzu group company, Japan) using a monochromatic Al Ka source (1486.6 eV). Isoelectric points of materials were measured by zeta potential analyzer (Malvern instruments limited, USA) as a function of pH.

2.4. Adsorption experiments

For adsorption kinetic studies, 100 mg of adsorbents were added to 200 mL aqueous solution with arsenic concentrations (100 mg L^{-1}) at natural pH, then the mixtures were shaken in a thermostatic oscillator and sampled at predetermined time intervals. The sorption isotherms were determined by adding 10 mg of adsorbents into 20 mL solution with arsenic concentrations ranging from 0.5 to 400 mg L^{-1} at natural pH. To investigate the effect of pH, the adsorption capacities at various pH values were determined after mixing 10 mg of adsorbents with 20 mL arsenic aqueous solution (50 mg L^{-1}) for 24 h, the pH values of the arsenic solution were adjusted with NaOH (0.1 M) or HCl (0.1 M). The influence of the competing ions and dissolved organic matter (DOM) was investigated by mixing anion NaCl, Na_2SO_4, $NaNO_3$, Na_2CO_3, Na_3PO_4, Na_2SiO_3 (1 mmol L^{-1}) and DOM (50 mg L^{-1}) with arsenic aqueous solution (50 mg L^{-1}) at natural pH, 10 mg of adsorbents was added to 20 mL mixed solution for 24 h. Considering the water solubility, fulvic acid (FA) was chosen as the DOM in this research. Batch adsorption experiments were carried out at in a platform shaker at room temperature (25 ± 1 °C) with a speed of 200 rpm. After experiment, the solution was filtered through a 0.45 mm filter and the residual concentrations of arsenic species were measured by inductively coupled plasma-atomic emission spectrometry (ICP-AES, IRIS Intrepid IIXSP).

2.5. Reusability and elution experiments

Arsenic-loaded samples were obtained by adding 100 mg MIL-101(Fe) into 200 mL solution containing 20 mg L^{-1} As(V). After adsorption equilibrium, the samples were collected by filtration and washed with de-ionized water. Then, following elution reagents were selected: 2 M NaCl, 10 mM HCl, 5 mM NaOH and 10 mM NaOH. Elution experiments were operated by adding 10 mg arsenic-loaded samples to 20 mL of the elution reagents. The mixtures were than shaken for 12 h at room temperature (25 °C) with a speed of 200 rpm. After selecting the most suitable reagent, the samples were filtered and dried for recycle used. The regeneration cycles were repeated for three times.

Toxicity Characteristic Leaching Procedure (TCLP) was operated following a previously reported method [40]. Extraction reagent was prepared by adding 64.3 mL of 1 M NaOH and 5.7 mL of glacial acetic acid to water, the solution was diluted to a final volume of 1L. The mixture containing arsenic-loaded samples and extraction reagents with the ratio of 1:20 was shaken for 18 h at room temperature (25 °C) with a speed of 200 rpm.

3. Results and discussion

3.1. Properties of MIL-101(Fe)

The surface morphology of MIL-101(Fe) nanoparticles was visualized with SEM and shown in Fig. 1(a). MIL-101(Fe) materials demonstrate the uniform octahedral structure with the diameter about 2 ∼ 3 μm, which is consistent with the previous study [38]. The as-synthesized MIL-101(Fe) was characterized by XRD in Fig. 1(b). The well-defined diffraction peaks located at 2θ of 5.25°, 5.99°, 8.57°, 9.19° and 16.54° confirm the formation of highly crystal MIL-101(Fe), which match well with the simulated MIL-101 [41] and other reported MIL-101(Fe) [42]. The nitrogen adsorption and desorption isotherms of MIL-101(Fe) shown in Fig. 1(c) exhibit type IV with H1 hysteresis loops behavior which are typical for mesoporous materials [43]. Previous report showed that two types of cages are presented in the framework of MIL-101, including microporous (∼8.6 Å) inside the super tetrahedra (ST) and mesoporous (∼29 Å and 34 Å) cages formed by adjacent ST [44]. It also be reflected by the pore size distribution (Fig. 1(c) inset) which shows that the percentages of macrospores, mesopores and micropores are 25.84%, 55.44% and 18.72%, respectively. The specific surface area calculated by BET method and the BJH pore volume are 1172.5 $m^2 g^{-1}$ and 1.16 $cm^3 g^{-1}$, respectively, which is larger than that of other reported Fe-BDC polymorphs including MIL-53(Fe) of 14 $m^2 g^{-1}$ and MIL-88(Fe) of 214 $m^2 g^{-1}$ [28,35], confirming the highly porosity of MIL-101(Fe). The result of thermo gravimetric analysis (TGA) shown in Fig. 1(d) demonstrates the excellent thermal stability of MIL-101(Fe) even at 300 °C in air. The weight loss (about 15%) below 350 °C may be attributed to the elimination of water molecular and free terephthalates in the pores of MIL-101 (Fe). Subsequently, the significant weight loss at temperature from 300 to 650 °C probably owe to the decomposition of coordinated organic ligands that result in the collapse of the framework, which is similar to the other MOFs formed by terephthalate ligand such as UIO-66 and MIL-101(Cr) [45,46].

3.2. Adsorption kinetics comparison of different arsenicals

Kinetic experiments were used to investigate the rate of arsenic removal from water by the adsorbent. Fig. 2(a) shows the adsorption kinetics of arsenic species onto MIL-101(Fe) particles. Similar trends of the variation of adsorption as a function of reaction time are presented for different types of arsenic. The adsorption of all the arsenic species on MIL-101(Fe) were fast at the beginning, and then sharply leveled off, the equilibrium time reached approximately after 4 h.

To analyze the adsorption kinetics precisely, pseudo-first-order (1) and pseudo-second-order (2) models were used to simulate the adsorption of arsenic species on MIL-101(Fe) particles [47], which can be expressed as follows:

$$Q_t = Q_e\left(1 - e^{-k_1 t}\right) \quad (1)$$

$$Q_t = \frac{k_2 Q_e^2 t}{1 + k_2 Q_e t} \quad (2)$$

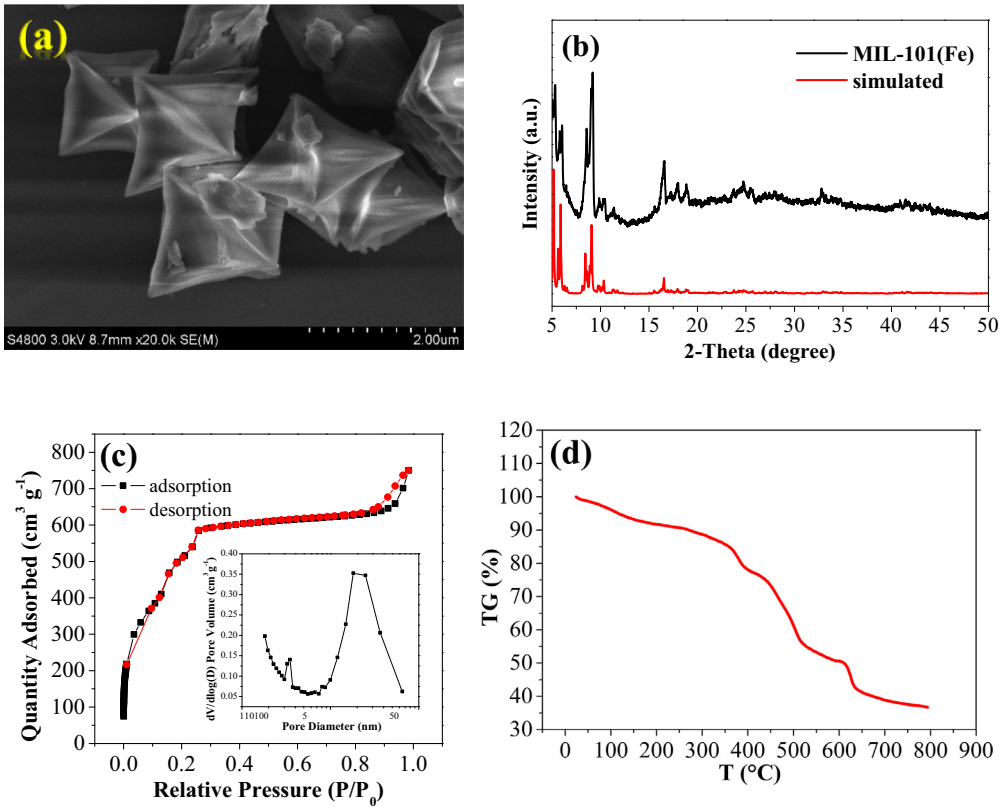

Fig. 1. (a) SEM image, (b) XRD patterns, (c) Nitrogen adsorption-desorption isotherms with pore size distribution (inset), and (d) Thermogravimetric curve of MIL-101(Fe).

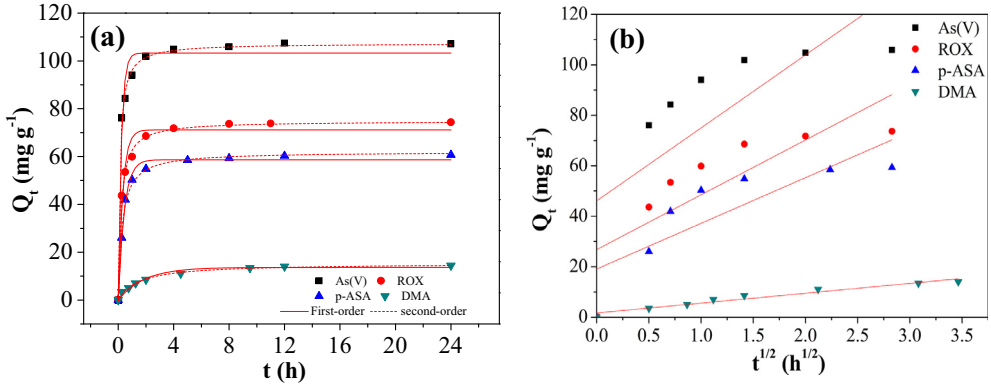

Fig. 2. (a) Adsorption kinetics of arsenic species on MIL-101(Fe) nanoparticles and (b) linear fittings of intraparticle diffusion model.

where Q_t (mg g^{-1}) and Q_e (mg g^{-1}) are the adsorption capacity at any time and at adsorption equilibrium, the parameter k_1 (h^{-1}) and k_2 (g mg^{-1}h^{-1}) are the first and second order kinetic rate constants, respectively.

As the calculated kinetic constants listed in Table 1, the adsorptions of all arsenic species were fitted better by the pseudo-second-order models with relatively high correlation coefficients ($R^2 > 0.98$). The adsorbed amounts obtained through the

Table 1
Kinetics parameters for adsorption.

	First-order			Second-order				Intraparticle diffusion		
	Q_e (mg g^{-1})	k_1 (h^{-1})	R^2	Q_e (mg g^{-1})	k_2 (g mg^{-1} h^{-1})	R^2	Experience Q_e (mg g^{-1})	k_p (mg g^{-1} h$^{-0.5}$)	C	R^2
As(V)	103.25	4.5021	0.9741	107.33	0.0805	0.9973	107.41	28.91	46.11	0.4637
ROX	71.1	3.0765	0.9683	74.84	0.0687	0.9973	74.31	21.72	26.80	0.5916
p-ASA	58.66	2.3126	0.9907	62.01	0.0577	0.9934	60.71	18.10	19.11	0.6316
DMA	13.66	0.5355	0.9649	15.33	0.0444	0.9884	14.42	3.91	1.67	0.9431

pseudo-second-order model are close to the experimental results, confirming that chemisorption is the dominant mechanism of the overall adsorption process[48]. Based on the k_2 value, the adsorption rates of different arsenic species are decreased in the following order: As(V) > ROX > p-ASA > DMA.

The rate controlling step and diffusion mechanism were investigated by using intraparticle diffusion model (3) based on the kinetic data before equilibrium [49].

$$Q_t = k_p t^{0.5} + C \quad (3)$$

where Q_t (mg g^{-1}) is the adsorption capacity at time t; k_p (mg $g^{-1}h^{-0.5}$) and C are the intraparticle diffusion rate constant and intercept, respectively.

Previous study found that three diffusion steps were involved in the entire adsorption process [49]: (i) arsenic molecules transferred across the external boundary layer of the adsorbent, (ii) intraparticle diffusion of arsenic occurred in the pores of the adsorbents and (iii) adsorption at sites on the surface. According to the hypothesis [50], the step (iii) usually occurred extremely rapid, thus the adsorption was assumed to be controlled by boundary layer diffusion or/and intraparticle diffusion. As the fitting results shown in Fig. 2(b) and Table 1, the plot of adsorption represents linear for DMA with relatively high correlation coefficient, indicating that intraparticle diffusion was the rate controlling process. On the contrary, the plots for As(V), ROX and p-ASA are not linear over the entire time range, implying that the adsorption were affected by both boundary layer diffusion and intraparticle diffusion. Moreover, the contribution of boundary layer diffusion is in direct proportion to the intercept (C) of the plots [51]. It is noteworthy that the C values follow the order As(V) > ROX > p-ASA > DMA, which is consistent with the order of adsorption rates, confirming that higher contribution of boundary layer diffusion would result in faster adsorption processes.

By inference, the diversity of adsorption rate and diffusion controlling step of arsenic species on MIL-101(Fe) is presumably caused by not only the variation of molecular structure but also the adsorption interaction of different arsenic species. Conventional Fe-based adsorbents usually showed higher adsorption rate for As(V) than organoarsenicals, such as $MnFe_2O_4$ [52], magnetite [53,54], ferrihydrite and goethite [55]. It could be explained by that Fe—O—As coordination was usually considered as the possible adsorption mechanism of arsenic onto Fe-based materials, the number of coordinative sites in arsenic species is depended on the amounts of the hydroxyl groups in their molecules. In general, As(V) have three hydroxyl groups that can offer four possible edge sites to form monodentate mononuclear complex and six possible sites to form bidentate binuclear complex with MIL-101(Fe); while ROX and p-ASA have two hydroxyl groups because of the substituted benzene ring that can offer three possible edge sites to from monodentate mononuclear complex and three possible sites to form bidentate binuclear complex with MIL-101(Fe) [56]. For DMA, one hydroxyl group is present in its molecular due to the substituted two methyl groups, thus it only has two possible sites to form monodentate mononuclear complex and one site to form bidentate complex with MIL-101(Fe) [57]. For this reason, higher amounts of coordinatively sites in As(V) will make it more easier to form any surface complexes, which results in adsorption rate higher than ROX, p-ASA and much higher than that of DMA. Considering the same coordination condition of ROX and p-ASA, the slightly higher adsorption rate of ROX than p-ASA might attribute to the difference of their functional groups in the aromatic rings. Previous study suggested that other interaction mechanism such as hydrogen bonding may occur between the organic linker in MOFs and the functional groups in organoarsenicals [27]. Therefore, the adsorption mechanisms of organoarsenicals onto MIL-101(Fe) are more complex than As(V), which will be detailed discussed in Section 3.5.

3.3. Adsorption isotherms comparison of different arsenicals

The adsorption isotherms experiments were operated to evaluate the uptake capacity of MIL-101(Fe) for different arsenic species. As shown in Fig. 3, when the adsorbent reaches saturation, the amount of the equilibrium adsorption capacity (Q_e) of different arsenic species decreases in the following order ROX > p-ASA > As(V) > DMA. Meanwhile, it is noteworthy that the Q_e of As(V) exceed the Q_e of ROX at relatively low initial concentration (C_0 <100 mg L^{-1}), which is similar to the results of kinetic analysis, indicating that substitution groups simultaneously affect the adsorption affinity and capacity of arsenate onto MIL-101(Fe).

This situation could be explained by the steric chemical structure diversity of different arsenic species. Previous results based on EXAFS suggest that the substituted benzene ring and dimethyl group in organoarsenicals result in larger molecular volume than that of As(V) [58,59]. Comparing the adsorption behaviors of As(V), ROX and p-ASA, when active sites in MIL-101(Fe) were sufficient for adsorption, the steric hindrance of organoarsenicals may affected their affinity with MIL-101(Fe) and led to lower adsorption capacity than that of As(V). When the adsorption sites of MIL-101(Fe) gradually became saturated with the increase of initial arsenic concentrations, ROX and p-ASA may form extra bonding with MIL-101(Fe) comparing with As(V), and subsequently synergistically increased the saturated adsorption capacity. Previous study suggested that p-ASA can interact with UIO-67 and NH_2-MIL-68 (In) through π-π stacking due to the presence of benzene ring in arsenic molecules and ligands on the MOFs [31,60]. Substituted —OH on the benzene ring of ROX and —NH_2 on p-ASA also enhance the adsorption via protonation reactions and forming hydrogen bond with the hydroxy group in the Fe-Mn binary oxide, respectively [61]. Thus, we speculate that the enhanced adsorption capacity of ROX and p-ASA at the high initial concentration (>100 mg L^{-1}) might be attributed to the extra adsorption mechanism including hydrogen bonding and π-π stacking. Aforementioned explanation can also be reflected in the previous study about adsorption of different arsenic species onto MOFs detailed in Table 2, the adsorption capacities of ROX and p-ASA reached 730.2 mg g^{-1} which are much higher than that of As(V) which generally less than 300 mg g^{-1}. It is noteworthy that when the initial As concentration below 1 mg L^{-1} (Fig. S1), although the C_e value of As(V), ROX and p-ASA were too low to compare their adsorption behavior, all of them were less than the permissive threshold value (10 μg L^{-1}) in drinking water limited by WHO, confirming the potential application of MIL-101(Fe) in the purification of arsenic-contaminated water.

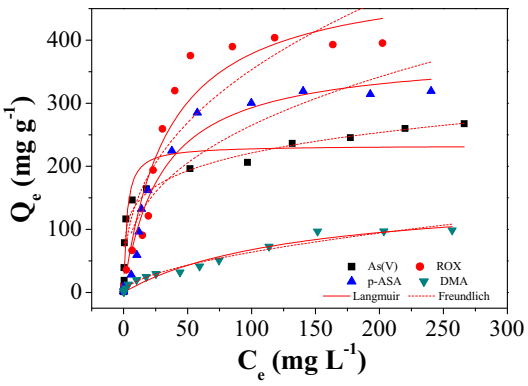

Fig. 3. Adsorption isotherm plots of arsenic adsorption on MIL-101(Fe).

Table 2
Comparing the adsorption capacities of arsenic species with other MOFs.

Adsorbent	Central ions	Arsenic adsorption capacity (mg g^{-1})				Reference
		As(V)	ROX	p-ASA	DMA	
NH_2-MIL-68(In)	In	–	–	503.2	–	[60]
ZIF-8	Zn	–	–	730.2	–	[64]
ZIF-8	Zn	60.2	–	–	–	[26]
Zn-MOF-74	Zn	325	–	–	–	[65]
MIL-101(Cr)	Cr	–	–	67.6	–	[27]
MIL-101(Cr)-$(OH)_3$	Cr	–	–	238.8	–	[27]
UiO-66	Zr	303.1	–	–	–	[66]
UiO-66	Zr	–	197.1	–	–	[67]
UIO-66-defect	Zr	–	729.8	–	–	[67]
UIO-67	Zr	–	–	455.3	–	[31]
UIO-67-NH_2(2)	Zr	–	–	179.5	–	[31]
MIL-53(Fe)	Fe	21.3	–	–	–	[28]
MIL-88A(Fe)	Fe	145.5	–	–	–	[29]
NH_2-MIL-88B(Fe)	Fe	125.2	–	–	–	[68]
MIL-100(Fe)	Fe	110	–	–	–	[34]
MIL-100(Fe)	Fe	–	387.3	366.0		[24]
Fe/Mg-MIL-88B	Fe/Mg	303.6	–	–	–	[69]
α-Fe_2O_3 derived from MIL-100(Fe)	Fe	182.7	–	–	–	[70]
MIL-101(Fe)	Fe	233.0	508.0	379.7	159.0	This study

The Q_e values of DMA in all the initial concentration ranges are much lower than that of other arsenic species, which is similar with the previous results for DMA adsorption on ferrihydrite, goethite [58] and aluminum oxide [62]. The cause of lower adsorption capacity for DMA is probably attributed to the presence of the substituted two methyl groups. Previous study suggested that the additional two methyl groups not only resulted in lower possible coordinative sites, but also may affected the molecular geometry of DMA, and consequently reduced its spatial compatibility with the surface adsorption sites of MIL-101(Fe) [57].

To obtain the maximum adsorption capacity, Langmuir (3) and Freundlich (4) isotherm models were used to analyze the adsorption equilibriums data [63], which can be expressed as follows:

$$Q_e = \frac{Q_m k_L C_e}{1 + k_L C_e} \tag{3}$$

$$Q_e = k_F C_e^{\,1/n} \tag{4}$$

where C_e (mg L^{-1}) and Q_e (mg g^{-1}) are the amount of the equilibrium concentration and equilibrium adsorption quantities, Q_m (mg g^{-1}) is the maximum adsorption quantities; k_L (L mg^{-1}) and k_F (mg g^{-1}) are constants of Langmuir and Freundlich model; n is the heterogeneity factor.

As shown in Table 3, the Q_e obtained from Langmuir model follow the order of ROX (507.97 mg g^{-1}) > p-ASA (379.65 mg g^{-1}) > As(V) (232.98 mg g^{-1}) > DMA (158.94 mg g^{-1}), which is corresponded to the experimental data and outperformed most of other reported MOFs (Table 2). Moreover, the loading dependent trends are well described by Freundlich the model for As(V), while fitted better by Langmuir model for ROX and p-ASA. In general, Langmuir isotherm model was used to describe the monolayer adsorption behavior that adsorbates homogeneously interact with the surface of adsorbents, while Freundlich isotherm model was based on the multilayer adsorption that involve the interaction between adsorbates each other. Previous studies suggested that the adsorption of As(V) onto MOFs involves two step. One is the direct binding of As (V) to the coordinatively unsaturated sites (CUSs) on the metal nodes, which is the dominated adsorption mechanism with fast adsorption kinetic. With the initial concentration of As(V) exceed the CUSs in MOFs, the free arsenate may interact with the adsorbed arsenate and form As—O—As coordination oligomers [23]. In case of DMA adsorption which is controlled by intraparticle diffusion due to the high steric hindrance, so DMA adsorption on MIL-101 (Fe) follows either Langmuir or Freundlich isotherm model. In comparison, the adsorption isotherms of ROX and p-ASA fit well with Langmuir isotherm model indicates that the adsorption sites are homogenous due to the hydrogen-bonding and π-π bonding adsorption interactions. Overall, MIL-101(Fe) is an efficient adsorbent for arsenate with high adsorption affinity and capacity. The substituted aromatic units in ROX and p-ASA enhance the adsorption capacity via the extra adsorption interaction, but inhibit the adsorption affinity due to the steric hindrance. The substituted two methyl groups in DMA significantly decrease both the adsorption capacity and affinity.

3.4. Effect of competing ions on different arsenicals on MIL-101(Fe)

As there are various anions which may compete with arsenic species during adsorption in aqueous environment. The effect of co-existing anionic ions (Cl^-, NO_3^-, SO_4^{2-}, CO_3^{2-}, SiO_3^{2-}, PO_4^{3-}) on different arsenic species adsorption are showed in Fig. 4. For all the arsenic species, inert electrolytes (Cl^-, NO_3^-, SO_4^{2-}) have slight effect on the adsorption capacities. Previous studies suggested that if the adsorbed ions forming outer-sphere with adsorbents locate at the same plane with electrolyte ions, the presence of electrolyte ions will inhibit the adsorption. In contrast, the inner-sphere complex

Table 3
Values of Freundlich and Langmuir Parameters.

	Langmuir			Freundlich		
	Q_{max} (mg g^{-1})	K_L (L mg^{-1})	R^2	K_F (mg g^{-1})	n	R^2
As(V)	232.98	0.4258	0.8595	89.23	5.0735	0.9636
ROX	507.97	0.0292	0.9119	58.14	2.6903	0.7979
p-ASA	379.65	0.0337	0.9538	48.79	2.7226	0.8318
DMA	158.94	0.0074	0.9454	4.82	1.7825	0.9684

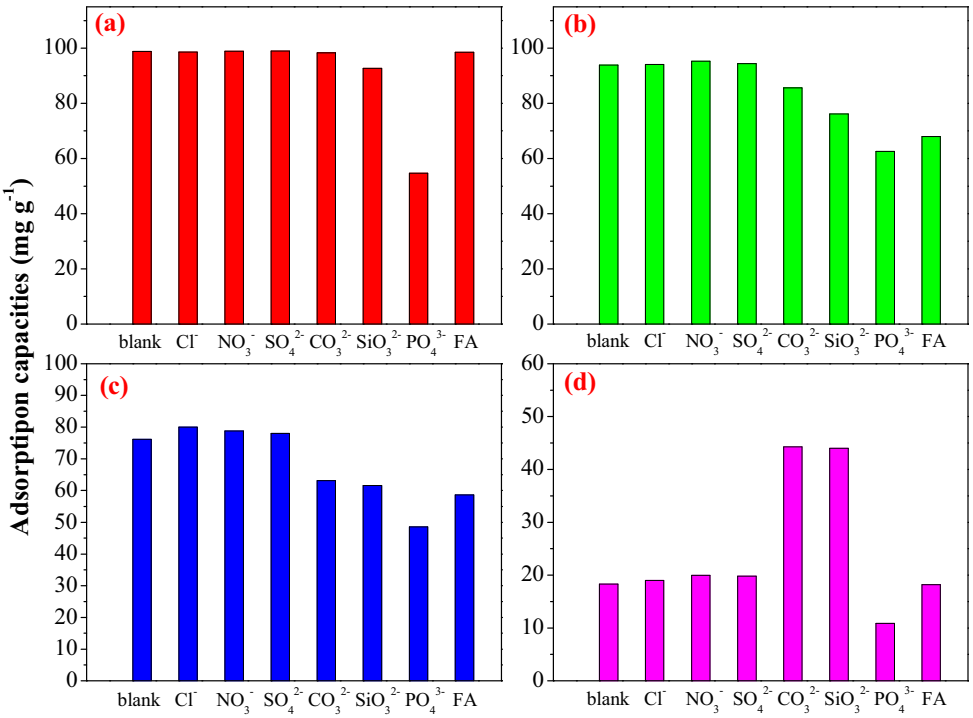

Fig. 4. Effect of competing anions of arsenic adsorption on MIL-101(Fe). (a) As(V), (b) ROX, (c) p-ASA and (d) DMA.

adsorption mechanism is hardly affected by electrolyte ions because the adsorbed ions directly coordinate to the surface metal atoms [40]. The point of zero charge (PZC) of MIL-101(Fe) before and after adsorption were also measured to identify the inner- or outer-sphere complexes, as specific adsorption (inner-sphere complexation) may change the PZC [59]. As shown in Fig. 5(a), the PZC of MIL-101(Fe) are shifted from 6.01 to 5.48, 3.60, 5.01 and 5.81 after loaded with As(V), ROX, p-ASA and DMA, respectively, indicating that inner-sphere complexes are formed between arsenic species and the adsorbent, which is consistent with results of $MnFe_2O_4$ and $CoFe_2O_4$ [71]. CO_3^{2-} and SiO_3^{2-} have no effect for the adsorption of As(V), implying that competitive adsorption is less likely to happen between arsenate and these two anions. However, the presence of CO_3^{2-} and SiO_3^{2-} slightly inhibit the adsorption of ROX and p-ASA, but obviously enhance the adsorption of DMA. Considering that both CO_3^{2-} and SiO_3^{2-} are strong weak acid salts, we speculate that the change of the amount of adsorbed ROX, p-ASA and DMA may due to the increasing basicity of the solution with the hydrolysis of these ions. Besides, the adsorption of all arsenic species is obviously inhibited by PO_4^{3-}. Arsenic and phosphorus are in the same main group, the highly similar atomic structures and chemical properties would make arsenate and phosphate easy to form inner-sphere complexes with the same active site of the adsorbents [72,73], thus the competitive adsorption between arsenic and phosphate may be attributed to the similar adsorption mechanism.

As dissolved organic matter (DOM) is considered as an important part in groundwater, fulvic acid (FA) was selected to investigate the effect of DOM on the adsorption. As shown in Fig. 4, the FA hardly affects the adsorption of As(V) and DMA, but moderately decreases the adsorption efficiency of ROX and p-ASA. Previous study demonstrated that DOM could be adsorbed onto the surface of MOFs via electrostatic interaction and π-π stacking interaction [74]. Thus, the decreasing adsorption capacities of ROX and p-ASA in the presence of FA might be attributed to the competitive sorption.

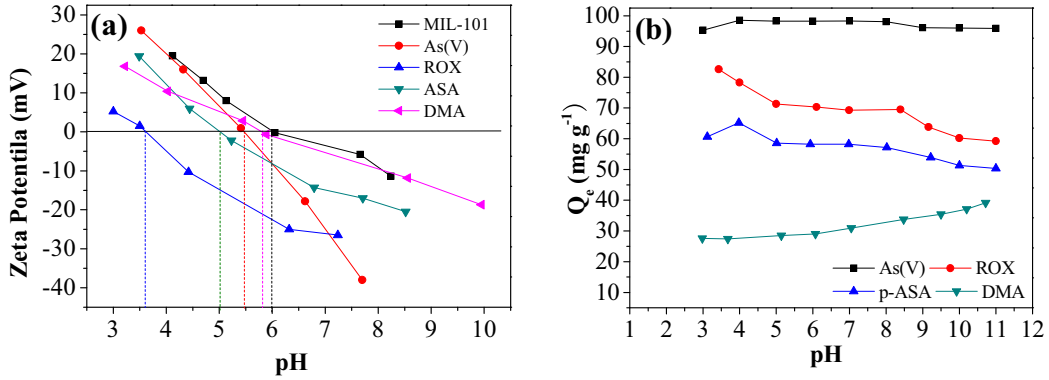

Fig. 5. (a) Zeta potentials of MIL-101(Fe) before and after arsenic species adsorption and (b) the effect of pH values on the adsorption of arsenic species.

3.5. Adsorption mechanism study

The results of adsorption behavior investigation suggest that the adsorption behaviors of different arsenic species are significantly affected by their chemical structure due to the variation of their adsorption mechanism. While chemisorption was proved the dominant adsorption for the adsorption of all arsenic species by the results of pseudo-second-order model fitting, in order to clarify how the chemical structure affect the adsorption process, possible mechanisms including electrostatic interaction, hydrogen bonding, coordination and π-π interaction will be discussed as follow [26,27].

3.5.1. Electrostatic interaction

To understand the contribution of electrostatic interaction more clearly, the amounts (Q_e) of arsenic species adsorbed over MIL-101 (Fe) were evaluated at pH range of 3 to 11 and the results are illustrated in Fig. 5(b). MIL-101(Fe) shows similar adsorption capacity of As(V) in the whole pH range. On the contrary, the adsorption of ROX, p-ASA and DMA are pH-dependent. The adsorption of ROX monotonically decreases with the increasing pH, the adsorption of p-ASA slightly enhances when pH increases from 3 to 4, and gradually declines till pH increases to 11. Adsorption of DMA increases with the increasing pH.

During the adsorption, both the surface charge of MIL-101(Fe) and the degree of ionization of arsenic species are affected by solution pH. The results of PZC shown in Fig. 5(a) show that the point of zero charge (PZC) of pristine MIL-101(Fe) approximately at pH of 6, implying that its surface charge should be positive below pH 6 or negative above pH 6, respectively. In Fig. S2, the aqueous dissociation constants (pK_a) of arsenic species suggest that As(V), ROX, p-ASA and DMA can form anionic species above pH of 2.2, 3.4, 4.1 and 6.1, respectively. If electrostatic interaction plays an important role in adsorption, the Q_t of all the arsenic species should be highest at pH of 6 and decline with the increasing pH because of the electrostatic repulsion between negatively charged MIL-101(Fe) and anionic arsenic species. However, the results shown in Fig. 5 are inconsistent with the expectation, indicating that electrostatic interaction is not the main mechanism for the adsorption of arsenic species onto MIL-101(Fe).

Previous studies reported that the adsorption capacities of As (V) onto MIL-53(Fe) and MIL-88A(Fe) are strongly pH-dependent because electrostatic interaction is involved in the adsorption as well as their relatively low stability [28,29]. The uptakes of As(V) onto ZIF-8 decreased sharply at acidic condition with the high releasing of Zn^{2+}, meanwhile the adsorption performance was dissatisfied under basic condition due to the anion repulsion [26]. Thus, the constant adsorption performance for As(V) in wide range of pH ($3 \sim 11$) reveal that the strong interaction between MIL-101 (Fe) and arsenate, indicating MIL-101(Fe) a promising adsorbent for arsenate removal. By comparison, the uptakes of ROX and p-ASA are slightly inhibited by the increasing pH, which means that the interaction is not strong enough to overcome the electrostatic repulsion. Considering the same adsorption mechanism of As(V) and DMA, the enhancement of DMA adsorption capacity with increasing pH may be attributed to that the free BDC occupying the pores dissolved in alkaline condition, thus the steric hindrance between DMA molecules and the adsorption sites should be relieved.

3.5.2. Coordination

Coordination is an important mechanism used to explain the adsorption of arsenic species over Fe-based materials because the bidentate binuclear, bidentate mononuclear and monodentate mononuclear complexes can occur between Fe—OH groups and As—O [52]. In the structure of MIL-101(Fe) with framework formula $Fe_3OCl(H_2O)_2(BDC)_3$ [75], each node is connected to three BDC linkers with terminal Cl^- or H_2O occupying the remaining three coordination sites. In theory, each cluster of MIL-101(Fe) has three coordinatively unsaturated sites (CUSs) that can act as Lewis acid sites and result in the formation of Fe—OH by deprotonation in aqueous solution [76]. Therefore, arsenic species would form Fe—O—As coordination by exchange the hydroxyl groups in Fe clusters of MIL-101(Fe). To demonstrate the role of coordination in the adsorption, XPS study was conducted to investigate the interaction between MIL-101(Fe) and arsenic species. As the XPS wide-scan spectra of MIL-101(Fe) shown in Fig. 6(a), the peaks located at 711.00, 531.00, 285.00 and 198.00 eV are assigned to the characteristic peaks of Fe2p, O 1s, C 1s and Cl 2p, respectively. After arsenic species adsorption, the peaks of As 3d, As 3p and As 2 s are detected, indicating the retention of arsenic species on MIL-101(Fe). In the high-resolution O 1s spectrum of pristine MIL-101(Fe) shown in Fig. 6(b), three peaks located at 530.41, 531.8 and 533.33 eV are related to O in iron oxide (Fe—O—Fe), iron bonded to hydroxyl/organic ligands (Fe—OH/Fe—O—C) and unbonded carboxyl (O—C=O), respectively [28,38]. After adsorption of As(V) and p-ASA, the area ratio of peak of O—C=O (533.33 eV) increases from 7.00% to 13.00% and 10.60%, respectively, indicating that the bonds between the Fe—O nodes and carboxylate in ligands may be partly broken during the adsorption, and resulting in the formation of free carboxylate groups. After adsorption of ROX, the proportion of peak at 533.33 eV increased to 37.70% in contrast to the pristine material, it may due to the presence of oxygen-containing groups in the benzene ring of ROX (C—OH/C—N=O) [67,77]. Considering this explanation, the area ratios of peak at 531.8 eV decrease from 84.00% to 26.45%, 23.70% and 24.20% after the adsorption of As(V), ROX and p-ASA, respectively, could be attributed to the decrease of amounts of Fe—OH during the adsorption. Combined with the completely disappearance of the peak at 530.41 eV, it is clearly to elucidate that the Fe—O—Fe and Fe—OH groups are involved in the adsorption process. Meanwhile, a strong new peak of Fe—O—As located at 530 ± 0.2 eV after adsorption [68], suggesting the significantly contribution of Fe—O—As coordination in the adsorption of arsenic species. Besides, not obvious difference in the O1s spectra are observed after the adsorption of DMA, the increase of the proportion of peak at 530.37 eV (from 9.00% to 19.70%) could be explained by the weak formation of Fe—O—As bond.

The FTIR spectra and of MIL-101(Fe) before and after adsorption are deconvoluted to further analyze the contribution of Fe—O—As coordination in the adsorption. As shown in Fig. 7, the broad peaks centered at 3366 cm^{-1} is corresponded to the stretching vibration of adsorbed water molecules. The broad band around 3100–3700 cm^{-1} is attributed to the H_2O and —OH groups in the material. The asymmetric and symmetric stretching vibration of O—C=O in carboxyl groups from BDC are showed at the peak about 1590 cm^{-1} and 1394 cm^{-1}, respectively, and the peak at 746 cm^{-1} is corresponded to the out-of-plane bending vibration of C—H in the aromatic ring of BDC [78]. The peak at 540 cm^{-1} is related to the stretching vibration of Fe—O [79]. After adsorption of As(V), ROX and p-ASA, the significant appearance of broad bands at 832 cm^{-1} assigned to the vibration of Fe—O—As proves the forming of strong inner-sphere surface complexes on MIL-101(Fe) surfaces [80], peaks intensities of ROX and p-ASA are weaker than As(V) though the adsorption quantities of these three arsenic species are roughly the same, suggesting that another mechanism may control the adsorption. Otherwise, the number and position of peaks among 1481 cm^{-1} to 1645 cm^{-1} which corresponded to the C=C stretching vibration of benzene ring are altered due to the difference of substituent group at ROX and p-ASA after adsorption [81]. It is notably that after adsorption of As(V), ROX and p-ASA, two new bands appear at 1280 cm^{-1} and 1686 cm^{-1}, which

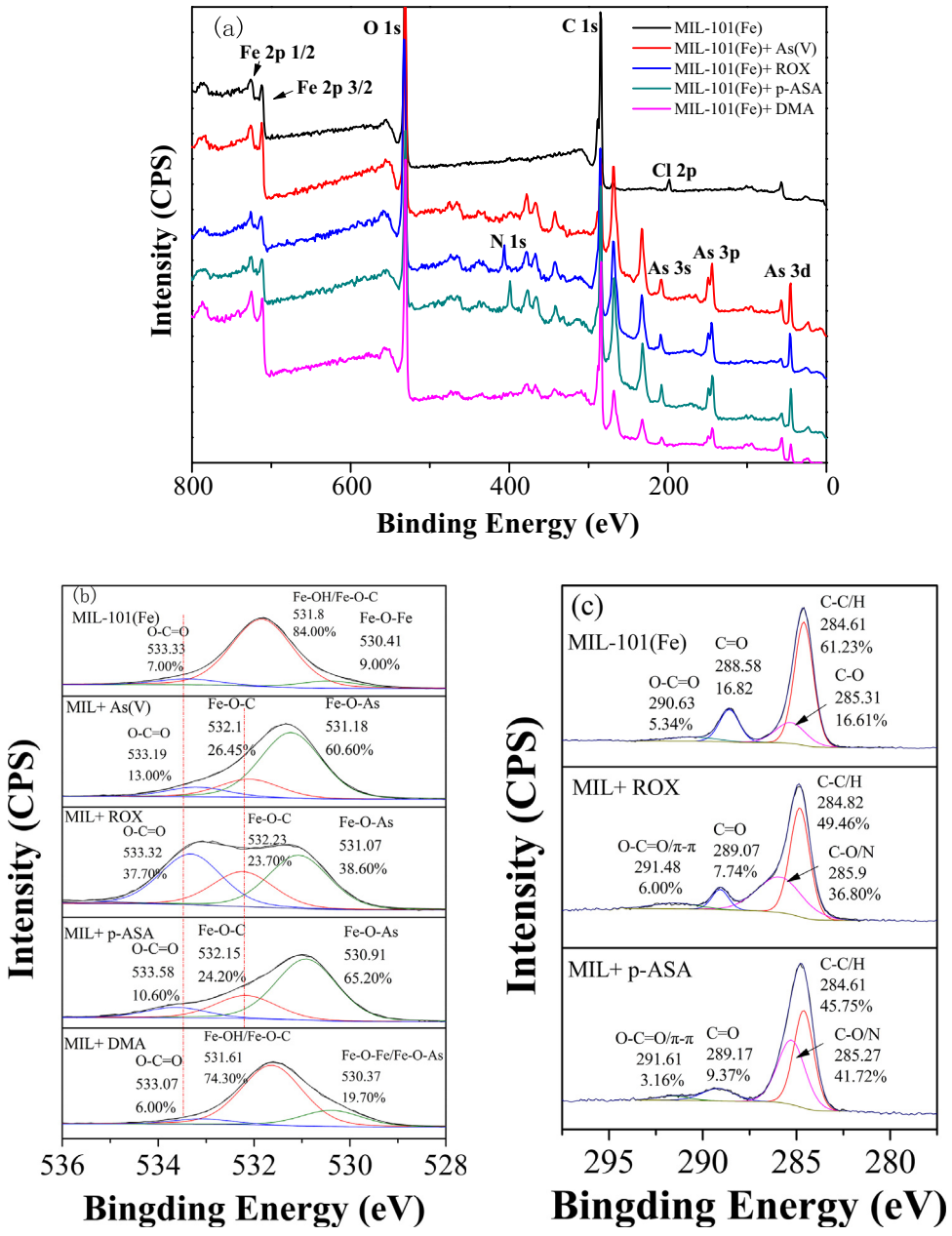

Fig. 6. XPS analysis of (a) wide scan, (b) O1s and (c) C1s of MIL-101(Fe) before and after adsorption.

might be attributed to the stretching vibration of C═O and C—OH of carboxyl groups, also confirming the slightly broken of Fe—O—C bond and the forming of unbonded carboxyl, which agrees with the results of XPS. Comparing with the other three arsenics, only one peak at 832 cm^{-1} enhance after the adsorption of DMA, suggesting that DMA bond to MIL-101(Fe) through forming Fe—O—As complexes without fracture the Fe—O—C connection. Above-mentioned results confirm the significant role of coordination in the adsorption.

3.5.3. Hydrogen bonding and π-π stacking interaction

According to the results of isotherm experiments, MIL-101(Fe) show higher adsorption capacities for ROX and p-ASA than As(V) although one of the hydroxy group has been replaced by aromatic unit, suggesting that another adsorption mechanism may occur between MIL-101(Fe) and the substitutional aromatic units. For the adsorption of aromatic organoarsenicals in MOFs according to previous study, hydrogen bonding is considered as an important adsorption mechanism because introducing —NH_2 in the ligand of MOFs can significantly enhance the adsorption capacity [31,60]. In order to confirm the existence of hydrogen bonding, the FTIR analysis of ROX and p-ASA were operated. As shown in Fig.S3, obvious peaks located at 3263 cm^{-1} in ROX and 3419 cm^{-1} in p-ASA are assigned to the —OH and —NH_2 groups, respectively. After adsorption (Fig. 7), no peak presented in 3263 cm^{-1} in the ROX loaded adsorbent, meanwhile the peak belonged to —NH_2 shifted to 3362 cm^{-1} in the p-ASA loaded adsorbent, indicating that the —OH and —NH_2 groups are involved in the adsorption. The FTIR results show that the strong Fe—O—As coordination leads to the generation of free —COOH through the ligand exchange. These carbonyl groups may form hydrogen bonds with the —NH_2 (C═O···H—N) in p-ASA and the —OH (C═O···H—O) in ROX, the hydroxyl groups also interact with —NH_2 in p-ASA by forming hydrogen bonds (O—H···N and O···H—N) [60]. Considering by this,

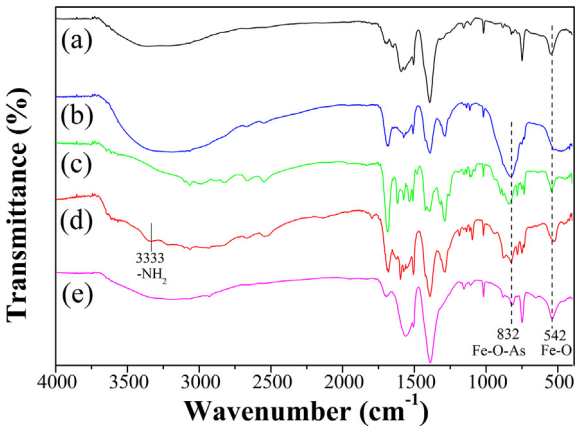

Fig. 7. FT-IR spectra of (a) pristine MIL-101(Fe) and after adsorption of (b) As(V), (c) ROX, (d) p-ASA and (e) DMA.

the decreasing adsorption capacity of p-ASA when pH less than 3 (Fig. 5(b)) could be interpreted as the situation where —NH_2 groups are gradually protonated at very low pH to form —NH_3^+ groups, according to the pK_a value of p-ASA (Fig. S2), which make p-ASA harder to form hydrogen bond with MIL-101(Fe) [27]. Moreover, the —NO_2 groups in p-ASA may enhance the hydrogen bonding. Xie et al. found that the high adsorption capacity of nitrobenzene in MIL-68-Al is attributed to the bonding between μ—OH in MOFs and the —NO_2 in nitrobenzene [82]. Another case about hydrogen-bonding based adsorption suggests that the much higher adsorption capacity of 4-nitrophenol (82.22 mg g^{-1}) than that of phenol (8.79 mg g^{-1}) is attributed to the strong electron withdrawing ability of —NO_2 groups that can reduce the overall electron density of aromatic units, and made 4-nitrophenol easier to form donor–acceptor complex with the ethylenediamine rosin-based resin than other phenol [83]. Such synergistic effect of —NO_2 and —OH in ROX may results in stronger hydrogen bond formation ability, which leads to relatively higher adsorption affinity and capacity of ROX onto MIL-101(Fe) than p-ASA.

In addition, previous results suggested that π-π stacking interaction play an important role in the adsorption of pollutants containing aromatic rings in MOFs [84–86]. Therefore, π-π stacking interaction, including face-to-face of face-to-edge orientations [87], is considered as another possible adsorption mechanism resulting in the higher adsorption capacities of aromatic organoarsenicals than As(V) due to the presence of benzene ring in the structure of aromatic organoarsenicals and the organic ligands of MIL-101(Fe). The π-π stacking interaction was evidenced with the high-resolution C 1 s XPS spectra shown in Fig. 6(c). For the pristine MIL-101(Fe), four peaks observed at 284.61, 285.31, 288.58 and 290.63 eV are assigned to the C—C/H, C—O, C═O and O—C═O groups in the organic ligands. After adsorption of ROX and p-ASA, the peak of MIL-101(Fe) located at 290.63 eV blue shift to 291.48 eV and 291.68 eV, respectively, which could be attributed to the generation of π-π component that appeared at 291.2 eV [88].

Based on aforementioned results and discussion, the main adsorption mechanism for arsenic species onto MIL-101(Fe) involves the following aspects and detailed in Scheme 1: (1) Fe—O—As coordination occurred between the hydroxyl groups in arsenic and coordinatively unsaturated sites in MIL-101(Fe), which is the predominant adsorption mechanism for As(V), ROX, p-ASA and DMA; (2) Hydrogen bonding interaction between the free —COOH and the substituent groups in benzene ring in ROX as well as p-ASA; (3) π-π stacking interaction between the aromatic units in ROX or ASA with BDC ligands in MIL-101(Fe).

In summary, MIL-101(Fe) presents excellent adsorption performance for arsenate benefiting by the strong Fe—O—As coordination, demonstrating the key role of central metal irons of MOFs in arsenic adsorption, which should be taken into consideration when apply MOFs for arsenic removal. Coordination, hydrogen bonding and π-π stacking interaction synergistically endow MIL-101(Fe) excellent adsorption capacities for ROX and p-ASA. However, the adsorption affinities for organoarsenicals are inhibited due to the steric hindrance from substituent groups, resulting in insufficient rate of adsorption comparing with As(V).

3.6. Stability and reusability of MIL-101(Fe)

As MIL-101(Fe) presents best adsorption performance for As(V), the stability and reusability of As(V) loaded adsorbent was investigated to evaluate the possible sustainable application of MIL-101 (Fe). The SEM image after adsorption of As(V) is shown in Fig. 8(a). MIL-101(Fe) remains the uniform octahedral structure morphology after adsorption, some arsenate species occupied the edges on MIL-101(Fe) and formed iron arsenate precipitation on the surface of MIL-101(Fe), resulting in the rough surface. Comparing with the pristine MIL-101(Fe), the structure was not change much, confirming the stability of MIL-101(Fe) after arsenic adsorption. However, the XRD pattern of MIL-101(Fe) after adsorption of As(V) shown in Fig. 8(b), almost all diffraction peaks disappear except the major peak at $2\theta = 9°$, indicating the reduced crystalline of MIL-101(Fe) during the adsorption. Previous study suggested that the strong diffraction peaks at low angles belong to the long-range order of uniform channels in the frameworks of MOFs. In this case, when arsenate diffuse into the channels, the strong Fe—O—As coordination may affect the inherent coordination between Fe clusters and BDC linkers, which may result in the partly broken of the long-range order of the framework and the reduced crystalline of MIL-101(Fe).

In order to investigate the reusability of MIL-101(Fe), several elution reagents including NaCl, HCl and NaOH were used to explore the elution experiment. As shown in Fig. 9(a), 2 M NaCl presents less than 2% elution efficiency, indicating that the adsorption of As(V) onto MIL-101(Fe) in neither though simple surface adsorption nor by forming outer-sphere complexes. When 10 mM HCl was used as elution reagent, only 30.34% elution efficiency can be observed, which is inconsistent with other reported Fe-based MOFs including MIL-100(Fe) and Fe/Mg-MIL-88(B) [34,69]. Combining with the result that the adsorption is stable even at pH = 3, we speculate that the MIL-101(Fe) can be used to immobilize arsenic. Thus, TCLP extraction procedure was further operated to predict the release of arsenic from MIL-101(Fe) [40]. As shown in Fig. 9(a), the TCLP leaching concentration of sample loaded 40 mg g^{-1} As(V) was only 3.8 mg L^{-1} (equal to 0.19% of elution efficiency), which did not exceed the maximum allowable leaching concentration of arsenic (5 mg g^{-1}) [89], implying the good immobilization of arsenic in MIL-101(Fe). Reliable elution efficiency (80.21%) can be observed when using 5 mM NaOH as elution reagent, the XRD pattern of sample after elution (green line) match well with the As(V) loaded sample (rad line), indicating that the loaded AsO_4^{3-} can be partly exchanged by —OH at certain concentration. Although all of the adsorbed As(V) can be eluted when the concentration of used NaOH was increased to 10 mM, the diffraction peaks of eluted sample (Fig. 6, blue line) completely disappear, it may due to the dissolve of acid organic linker and the subsequently decomposing framework structure [28].

As shown in Fig. 9(b), the samples eluted by 5 mM NaOH can only give 60% adsorption efficiency for As(V) after repeating for three times, implying that the reusability of MIL-101(Fe) are significantly affected by its disordered framework structure after arsenic adsorption. As discussed above, although the strong interaction between MIL-101(Fe) and arsenic results in the excellent adsorp-

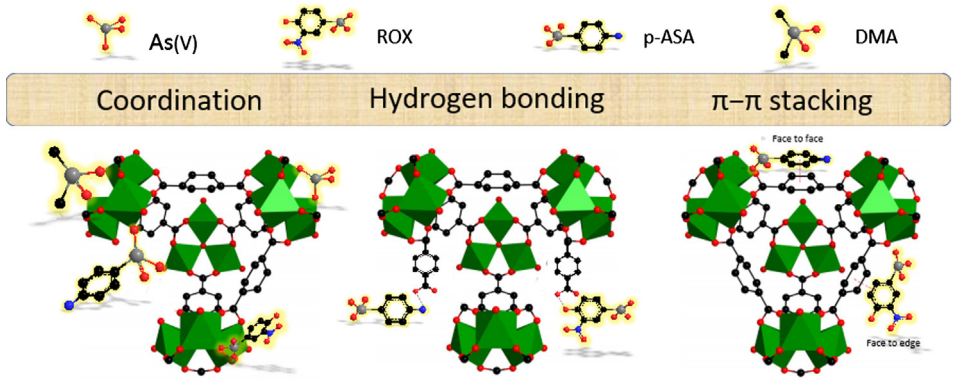

Scheme 1. Adsorption mechanisms of arsenic species on MIL-101(Fe). Fe_3 nodes, carbon, oxygen, arsenic and nitrogen atoms are shown in green, black, rad, gray and blue, respectively.

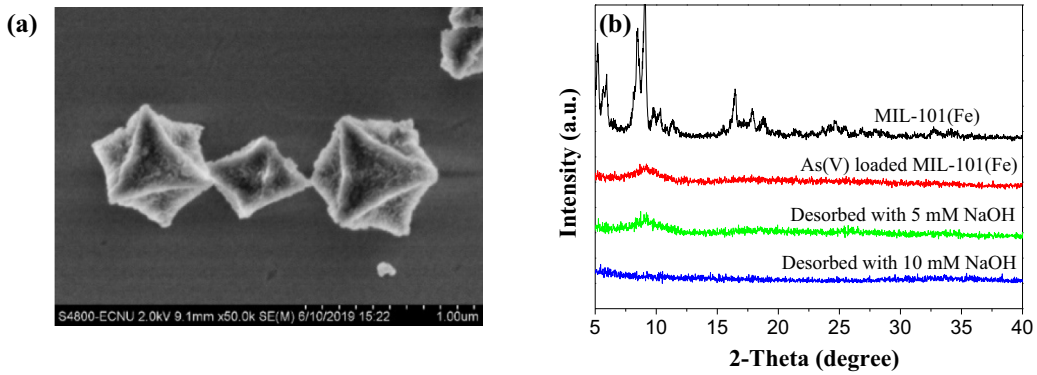

Fig. 8. The (a) SEM image of MIL-101(Fe) after As(V) adsorption and (b) XRD patterns of pristine samples, after loading As(V) and after elution by NaOH at different concentration.

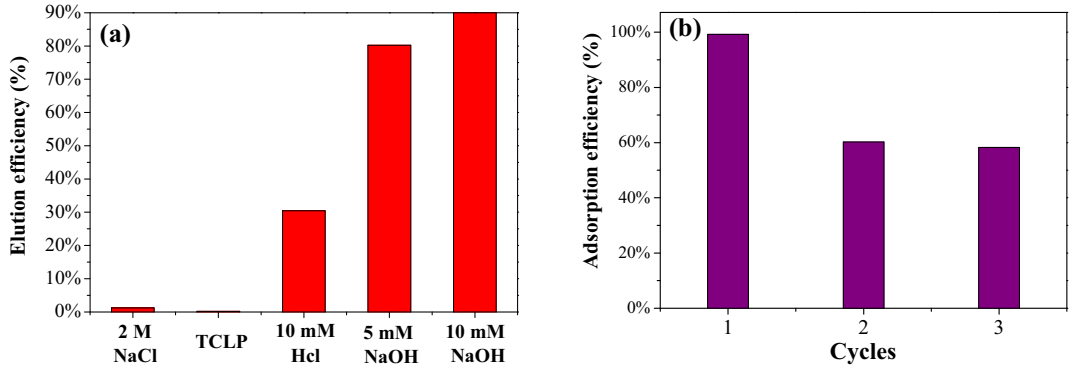

Fig. 9. (a) The elution efficiency by different elution solutions and (b) the removal rate of As(V) on MIL-101(Fe) under different regeneration cycles.

tion performance, the stability and reusability still significant challenges for designing Fe-based MOFs for arsenic removal.

4. Conclusions

In conclusion, Fe-based metal-organic framework MIL-101 (Fe) synthesized via a facile solvothermal method was firstly applied for the adsorption of arsenic species, and the effect of chemical structure of arsenate was emphasized on. Kinetic and isotherm studies showed that MIL-101(Fe) can adsorb As (V), ROX, p-ASA and DMA with excellent adsorption rate and capacities. Adsorption mechanism based on FTIR and XPS results suggested that the Fe—O—As coordination between arsenate and the incomplete-coordinated cationic Fe in the cluster is the primary adsorption mechanism for all the arsenic species. Substituent aromatic units in ROX and p-ASA strengthen the adsorption on MIL-101(Fe) through hydrogen bonds and π-π stacking interaction, resulting in higher adsorption capacities far beyond that of As(V) and DMA. The deep explanation of the role of arsenic chemical structural on adsorption on MIL-101(Fe) is still highly desired by X-ray Absorption Fine Structure analysis. However, the strong Fe—O—As coordination limits the reusability of MIL-101(Fe). Overall, this study confirms the potential value of MIL-101(Fe) as remarkable adsorbent to control the aqueous arsenic contamination. Arsenic speciation has significant impact on adsorption, which should be taken in consideration when apply adsorbents in arsenic removal.

Acknowledgements

We appreciate the support from the Shanghai natural science foundation of China (no. 19ZR1414900) and National Natural Science Foundation of China (no. 21377039).

Appendix A. Supplementary material

Supplementary data to this article can be found online at https://doi.org/10.1016/j.jcis.2019.07.046.

References

[1] A.J. Bednar, J.R. Garbarino, J.F. Ranville, T.R. Wildeman, Presence of organoarsenicals used in cotton production in agricultural water and soil of the Southern United States, J. Agric. Food. Chem. 50 (25) (2002) 7340–7344.
[2] S. Zheng, W. Jiang, Y. Cai, D.D. Dionysiou, K.E. O'Shea, Adsorption and photocatalytic degradation of aromatic organoarsenic compounds in TiO_2 suspension, Catal. Today 224 (2014) 83–88.
[3] F. Jones, A broad view of arsenic, Poultry Sci. 86 (1) (2007) 2–14.
[4] S. Kumar, R.R. Nair, P.B. Pillai, S.N. Gupta, M.A. Iyengar, A.K. Sood, Graphene oxide–$MnFe_2O_4$ magnetic nanohybrids for efficient removal of lead and arsenic from water, ACS Appl. Mater. Interf. 6 (20) (2014) 17426–17436.
[5] L. Wang, H. Cheng, Birnessite (δ-MnO_2) mediated degradation of organoarsenic feed additive p-arsanilic acid, Environ. Sci. Technol. 49 (6) (2015) 3473–3481.
[6] A. Basu, D. Saha, R. Saha, T. Ghosh, B. Saha, A review on sources, toxicity and remediation technologies for removing arsenic from drinking water, Res. Chem. Intermed. 40 (2) (2014) 447–485.
[7] D. Mohan, C.U. Pittman Jr, Arsenic removal from water wastewater using adsorbents—a critical review, J. Hazard. Mater. 142 (1–2) (2007) 1–53.
[8] K. Jomova, Z. Jenisova, M. Feszterova, S. Baros, J. Liska, D. Hudecova, C.J. Rhodes, M. Valko, Arsenic: toxicity, oxidative stress and human disease, J. Appl. Toxicol. 31 (2) (2011) 95–107.
[9] C.J. Chen, H.Y. Chiou, W.I. Huang, S.Y. Chen, Y.M. Hsueh, C.H. Tseng, L.J. Lin, M.P. Shyu, M.S. Lai, Systemic non-carcinogenic effects and developmental toxicity of inorganic arsenic, Arsenic Springer, Dordrecht, 1997, p. 134.
[10] S.R. Wickramasinghe, B. Han, J. Zimbron, Z. Shen, M.N. Karim, Arsenic removal by coagulation and filtration: comparison of groundwaters from the United States and Bangladesh, Desalination 169 (3) (2004) 231–244.
[11] F.G. Vagliasindi, M.M. Benjamin, Arsenic removal in fresh and nom-preloaded ion exchange packed bed adsorption reactors, Water Sci. Technol. 38 (6) (1998) 337–343.
[12] K. Jaworek, M. Czaplicka, Decomposition of phenylarsonic acid by AOP processes: degradation rate constants and by-products, Environ. Sci. Pollution Res. 21 (20) (2014) 11917–11923.
[13] R.R. Nidia, H.R. Laura, G.M.J. Luis, C. Yong, O.S. Kevin, H.-R. Aracely, Photocatalytical removal of inorganic and organic arsenic species from aqueous solution using zinc oxide semiconductor, Photochem. Photobiolog. Sci. 12 (4) (2013) 653–659.
[14] A. Byungryul, Z. Dongye, Immobilization of As (III) in soil and groundwater using a new class of polysaccharide stabilized Fe-Mn oxide nanoparticles, J. Hazard. Mater. 211 (2012) 332–341.
[15] J. Pattanayak, K. Mondal, S. Mathew, S. Lalvani, A parametric evaluation of the removal of As (V) and As (III) by carbon-based adsorbents, Carbon 38 (4) (2000) 589–596.
[16] B. Luke, M. Marta, The immobilisation and retention of soluble arsenic, cadmium and zinc by biochar, Environ. Pollut. 159 (2) (2011) 474–480.
[17] X. Guan, J. Du, X. Meng, Y. Sun, B. Sun, Q. Hu, Application of titanium dioxide in arsenic removal from water: a review, J. Hazard. Mater. 215 (2012) 1–16.
[18] J. Hu, Z. Tong, Z. Hu, G. Chen, T. Chen, Adsorption of roxarsone from aqueous solution by multi-walled carbon nanotubes, J. Colloid Interf. Sci. 377 (1) (2012) 355–361.
[19] L. Poon, S. Younus, L.D. Wilson, Adsorption study of an organo-arsenical with chitosan-based sorbents, J. Colloid Interf. Sci. 420 (2014) 136–144.
[20] R. Hamed, M. Faranak, Synthesis of a novel MOF/$CuWO_4$ heterostructure for efficient photocatalytic degradation and removal of water pollutants, J. Cleaner Prod. 172 (2018) 2655–2666.
[21] J. Li, Z. Wu, Q. Duan, A. Ahmed, T. Hayat, C. Chen, Decoration of ZIF-8 on polypyrrole nanotubes for highly efficient and selective capture of U (VI), J. Cleaner Prod. 204 (2018) 896–905.
[22] Z. Moeini, A. Azhdarpoor, S. Yousefinejad, H. Hashemi, Removal of atrazine from water using titanium dioxide encapsulated in salicylaldehyde-NH_2-MIL-101(Cr): adsorption or oxidation mechanism, J. Cleaner Prod. 224 (2019) 238–245.
[23] C.O. Audu, H.G. Nguyen, C.Y. Chang, M.J. Katz, L. Mao, O.K. Farha, J.T. Hupp, S.T. Nguyen, The dual capture of As(V) and As(III) by UiO-66 and analogues, Chem. Sci. 7 (10) (2016) 6492–6498.
[24] J.W. Jun, M. Tong, B.K. Jung, Z. Hasan, C. Zhong, S.H. Jhung, Effect of central metal ions of analogous metal–organic frameworks on adsorption of organoarsenic compounds from water: plausible mechanism of adsorption and water purification. Chemistry–A, Eur. J. 21 (1) (2015) 347–354.
[25] X. Zhu, B. Li, J. Yang, Y. Li, W. Zhao, J. Shi, J. Gu, Effective adsorption and enhanced removal of organophosphorus pesticides from aqueous solution by Zr-based MOFs of UiO-67, ACS Appl. Mater. Interf. 7 (1) (2014) 223–231.
[26] M. Jian, B. Liu, G. Zhang, R. Liu, X. Zhang, Adsorptive removal of arsenic from aqueous solution by zeolitic imidazolate framework-8 (ZIF-8) nanoparticles, Coll. Surf. A 465 (2015) 67–76.
[27] M. Sarker, J.Y. Song, S.H. Jhung, Adsorption of organic arsenic acids from water over functionalized metal-organic frameworks, J. Hazard. Mater. 335 (2017) 162–169.
[28] T.A. Vu, G.H. Le, C.D. Dao, L.Q. Dang, K.T. Nguyen, Q.K. Nguyen, P.T. Dang, H.T. Tran, Q.T. Duong, T.V. Nguyen, G.D. Lee, Arsenic removal from aqueous solutions by adsorption using novel MIL-53(Fe) as a highly efficient adsorbent, Rsc Adv. 5 (7) (2015) 5261–5268.
[29] H. Wu, M. Ma, W. Gai, H. Yang, J. Zhou, Z. Cheng, P. Xu, Z. Deng, Arsenic removal from water by metal-organic framework MIL-88A microrods, Environ. Sci. Pollut. Res. 25 (27) (2018) 27196–27202.
[30] Z.Q. Li, J.C. Yang, K.W. Sui, N. Yin, Facile synthesis of metal-organic framework MOF-808 for arsenic removal, Mater. Lett. 160 (2015) 412–414.
[31] T. Chen, J. Zhao, X. Ou, J. Wan, Y. Cai, Z. Lin, Z. Dang, B. Xing, Enhanced adsorption of p-arsanilic acid from water by aminemodified UiO-67 as examined using extended X-ray absorption fine structure X-ray photoelectron spectroscopy, and density functional theory calculations, Environ. Sci. Technol. 52 (6) (2018) 3466–3475.
[32] Q. Hu, Y. Liu, e.a. Gu X, Adsorption behavior and mechanism of different arsenic species on mesoporous $MnFe_2O_4$ magnetic nanoparticles, Chemosphere 181 (2017) 328–336.
[33] D. Fu, Z. He, S. Su, B. Xu, Y. Liu, Y. Zhao, Fabrication of α-FeOOH decorated graphene oxide-carbon nanotubes aerogel and its application in adsorption of arsenic species, J. Coll. Interf. Sci. 505 (2017) 105–114.
[34] J. Cai, X. Wang, Y. Zhou, L. Jiang, C. Wang, Selective adsorption of arsenate and the reversible structure transformation of the mesoporous metal–organic framework MIL-100(Fe), Phys. Chem. Chem. Phys. 18 (16) (2016) 10864–10867.
[35] S. Hou, Y. Wu, L. Feng, W. Chen, Y. Wang, C. Morlay, F. Li, Green synthesis and evaluation of an iron-based metal–organic framework MIL-88B for efficient decontamination of arsenate from water, Dalton Trans. 47 (7) (2018) 2222–2231.
[36] A. Miroslav, Z. Vladimír, P. Peter, B. Eva, Z. Adriana, Metal-organic framework MIL-101(Fe)-NH_2 functionalized with different long-chain polyamines as drug delivery system, Inorg. Chem. Commun. 93 (2018) 115–120.
[37] F. Carson, J. Su, A.E. Platero-Prats, W. Wan, Y. Yun, L. Samain, X. Zou, Framework isomerism in vanadium metal–organic frameworks: MIL-88B(V) and MIL-101(V), Crystal growth and design 13 (11) (2013) 5036–5044.
[38] Q. Xie, Y. Li, Z. Lv, H. Zhou, X. Yang, J. Chen, H. Guo, Effective adsorption and removal of phosphate from aqueous solutions and eutrophic water by Fe-based MOFs of MIL-101, Sci. Rep. 7 (1) (2017) 3316.
[39] N.V. Maksimchuk, K.A. Kovalenko, V.P. Fedin, O. Kholdeeva, Cyclohexane selective oxidation over metal–organic frameworks of MIL-101 family superior catalytic activity and selectivity, Chem. Commun. 48 (54) (2012) 6812–6814.
[40] A.C. Ladeira, V.S. Ciminelli, Adsorption and desorption of arsenic on an oxisol and its constituents, Water Research 38 (8) (2004) 2087–2094.
[41] F. Gerard, M.-D. Caroline, S. Christian, M. Franck, D. Julien, S. Suzy, M. Irena, A chromium terephthalate-based solid with unusually large pore volumes and surface area, Science 309 (5743) (2005) 2040–2042.
[42] X. Li, W. Guo, Z. Liu, R. Wang, H. Liu, Quinone-modified NH_2-MIL-101(Fe) composite as a redox mediator for improved degradation of bisphenol A, J. Hazard. Mater. 324 (2017) 665–672.
[43] Y. Li, Z. Yang, Y. Wang, Z. Bai, T. Zheng, X. Dai, S. Liu, D. Gui, W. Gui, M. Chen, A mesoporous cationic thorium-organic framework that rapidly traps anionic persistent organic pollutants, Nat. Commun. 8 (1) (2017) 1354-1364.
[44] O. Lebedev, F. Millange, C. Serre, G. Van Tendeloo, G. Férey, First direct imaging of giant pores of the metal− organic framework MIL-101, Chem. Mater. 17 (26) (2005) 6525–6527.
[45] Z. Hu, M. Khurana, Y.H. Seah, M. Zhang, Z. Guo, D. Zhao, Ionized Zr-MOFs for highly efficient post-combustion CO_2 capture, Chem. Eng. Sci. 124 (2015) 61–69.
[46] C.X. Yang, X.P. Yan, Metal-organic framework MIL-101(Cr) for high-performance liquid chromatographic separation of substituted aromatics, Anal. Chem. 83 (18) (2011) 7144–7150.
[47] Y.S. Ho, G. McKay, Pseudo-second order model for sorption processes, Process Biochem. 34 (5) (1999) 451–465.
[48] Y.S. Ho, G. McKay, The kinetics of sorption of divalent metal ions ontosphagnum moss peat, Water Res. 34 (3) (2000) 735–742.
[49] K.K. Vasanth, P.K. Mass, transfer, kinetics and equilibrium studies for the biosorption of methylene blue using Paspalum notatum, J. Hazard. Mater. 146 (1–2) (2007) 214–226.
[50] W.H. Cheung, Y.S. Szeto, G. McKay, Intraparticle diffusion processes during acid dye adsorption onto chitosan, Bioresource Technol. 98 (15) (2007) 2897–2904.
[51] M. Sankar, G. Sekaran, S. Sadulla, T. Ramasami, Removal of diazo and triphenylmethane dyes from aqueous solutions through an adsorption process, J. Chem. Technol. Biotechnol.: Int. Res Process, Environ. Clean Technol. 74 (4) (1999) 337–344.
[52] Q. Hu, Y. Liu, X. Gu, Y. Zhao, Adsorption behavior and mechanism of different arsenic species on mesoporous $MnFe_2O_4$ magnetic nanoparticles, Chemosphere 181 (2017) 328–336.

[53] L. Feng, M. Cao, X. Ma, Y. Zhu, C. Hu, Superparamagnetic high-surface-area Fe_3O_4 nanoparticles as adsorbents for arsenic removal, J. Hazard. Mater. 217 (2012) 439–446.
[54] C. Tian, J. Zhao, J. Zhang, S. Chu, Z. Dang, Z. Lin, B. Xing, Enhanced removal of roxarsone by Fe_3O_4@3D graphene nanocomposites synergistic adsorption and mechanism, Environ. Sci. Nano 4 (11) (2017) 2134–2143.
[55] J. Zhang, R. Stanforth, S. Pehkonen, Effect of replacing a hydroxyl group with a methyl group on arsenic (V) species adsorption on goethite (α-FeOOH), J. Coll. Interf. Sci. 306 (1) (2007) 16–21.
[56] W.R. Chen, C.H. Huang, Surface adsorption of organoarsenic roxarsone and arsanilic acid on iron and aluminum oxides, J. Hazard. Mater. 227 (2012) 378–385.
[57] B.J. Lafferty, R. Loeppert, Methyl Arsenic Adsorption and Desorption Behavior on Iron Oxides, Environ. Sci. Technol. 39 (7) (2005) 2120–2127.
[58] M. Shimizu, Y. Arai, D.L. Sparks, Multiscale assessment of methylarsenic reactivity in soil. 1. sorption and desorption on soils, Environ. Sci. Technol. 45 (10) (2011) 4293–4299.
[59] Y. Arai, E.J. Elzinga, D.L. Sparks, X-ray absorption spectroscopic investigation of arsenite and arsenate adsorption at the aluminum oxide-water interface, J. Coll. Interf. Sci. 235 (1) (2001) 80–88.
[60] Y. Lv, R. Zhang, S. Zeng, K. Liu, S. Huang, Y. Liu, P. Xu, C. Lin, Y. Cheng, M. Liu, Removal of p-arsanilic acid by an amino-functionalized indium-based metal–organic framework: Adsorption behavior and synergetic mechanism, Chem. Eng. J. 339 (2018) 359–368.
[61] T.P. Joshi, G. Zhang, W.A. Jefferson, A.V. Perfilev, R. Liu, H. Liu, J. Qu, Adsorption of aromatic organoarsenic compounds by ferric and manganese binary oxide and description of the associated mechanism, Chem. Eng. J. 309 (2017) 577–587.
[62] S. Masayuki, G.V. Matthew, S.J. Parikh, D.L. Sparks, Molecular scale assessment of methylarsenic sorption on aluminum oxide, Environ. Sci. Technol. 44 (2) (2009) 612–617.
[63] K.M. Alotaibi, L. Shiels, L. Lacaze, T.A. Peshkur, P. Anderson, L. Machala, K. Critchley, S.V. Patwardhan, L.T. Gibson, Iron supported on bioinspired green silica for water remediation, Chem. Sci. 8 (1) (2017) 567–576.
[64] B.K. Jung, J.W. Jun, Z. Hasan, S.H. Jhung, Adsorptive removal of p-arsanilic acid from water using mesoporous zeolitic imidazolate framework-8, Chem. Eng. J. 267 (2015) 9–15.
[65] W. Yu, M. Luo, Y. Yang, H. Wu, W. Huang, K. Zeng, F. Luo, Metal-organic framework (MOF) showing both ultrahigh As(V) and As(III) removal from aqueous solution, J. Solid State Chem. 269 (2019) 264–270.
[66] C. Wang, X. Liu, J.P. Chen, K. Li, Superior removal of arsenic from water with zirconium metalorganic framework UiO-66, Sci. Rep. 5 (2015) 16613.
[67] B. Li, X. Zhu, K. Hu, Y. Li, J. Feng, J. Shi, J. Gu, Defect creation in metal-organic frameworks for rapid and controllable decontamination of roxarsone from aqueous solution, J. Hazard. Mater. 302 (2016) 57–64.
[68] D. Xie, X. Yue, Y. Gu, H. Zhou, H. Zhang, G. Wang, Y. Zhang, H. Zhao, Bifunctional NH_2-MIL-88(Fe) metal–organic framework nanooctahedra for highly sensitive detection and efficient removal of arsenate in aqueous media, J. Mater. Chem. A 5 (45) (2017) 23794–23804.
[69] Y. Gu, D. Xie, Y. Wang, W. Qin, H. Zhang, G. Wang, Y. Zhang, H. Zhao, Facile fabrication of composition-tunable Fe/Mg bimetal-organic frameworks for exceptional arsenate removal, Chem. Eng. J. 357 (2019) 579–588.
[70] Z. Liu, J. Chen, Y. Wu, Y. Li, J. Zhao, P. Na, Synthesis of magnetic orderly mesoporous α-Fe_2O_3 nanocluster derived from MIL-100(Fe) for rapid and efficient arsenic(III, V) removal, J. Hazard. Mater. 343 (2018) 304–314.
[71] S. Zhang, H. Niu, Y. Cai, X. Zhao, Y. Shi, Arsenite and arsenate adsorption on coprecipitated bimetal oxide magnetic nanomaterials: $MnFe_2O_4$ and $CoFe_2O_4$, Chem. Eng. J. 158 (3) (2010) 599–607.
[72] A. Jain, R.H. Loeppert, Effect of competing anions on the adsorption of arsenate and arsenite by ferrihydrite, J. Environ. Quality 29 (5) (2000) 1422–1430.
[73] C. Su, R.W. Puls, Arsenate and arsenite removal by zerovalent iron: kinetics, redox transformation, and implications for in situ groundwater remediation, Environ. Sci. Technol. 35 (7) (2001) 1487–1492.
[74] K.Y.A. Lin, H.A. Chang, Efficient Adsorptive Removal of Humic Acid from Water Using Zeolitic Imidazole Framework-8 (ZIF-8), Water, Air and Soil Pollution 226 (2) (2015) 10-26.
[75] K.M. Taylor-Pashow, J. Della Rocca, Z. Xie, S. Tran, W. Lin, Postsynthetic modifications of iron-carboxylate nanoscale metal– organic frameworks for imaging and drug delivery, J. Am. Chem. Soc. 131 (40) (2009) 14261–14263.
[76] D.Y. Hong, Y.K. Hwang, C. Serre, G. Ferey, J.S. Chang, Porous chromium terephthalate MIL-101 with coordinatively unsaturated sites surface functionalization, encapsulation, sorption and catalysis, Adv. Funct. Mater. 19 (10) (2009) 1537–1552.
[77] S.F. Lim, Y.M. Zheng, J.P. Chen, Organic Arsenic Adsorption onto a Magnetic Sorbent, Langmuir 25 (9) (2009) 4973–4978.
[78] X. Yue, W. Guo, X. Li, H. Zhou, R. Wang, Core-shell Fe_3O_4@MIL-101(Fe) composites as heterogeneous catalysts ofpersulfate activation for the removal of acid orange 7, Environ. Sci. Pollut. Res. 23 (15) (2016) 15218–15226.
[79] Z. Zhang, X. Li, B. Liu, Q. Zhao, G. Chen, Hexagonal microspindle of NH_2-MIL-101(Fe) metal–organic frameworks with visible-light-induced photocatalytic activity for the degradation of toluene, RSC Adv. 6 (6) (2016) 4289–4295.
[80] G. Zhang, J. Qu, H. Liu, R. Liu, R. Wu, Preparation and evaluation of a novel Fe–Mn binary oxide adsorbent for effective arsenite removal, Water Res. 41 (9) (2007) 1921–1928.
[81] T.A. Vu, G.H. Le, C.D. Dao, L.Q. Dang, K.T. Nguyen, P.T. Dang, H.T. Tran, Q.T. Duong, T.V. Nguyen, G.D. Lee, Isomorphous substitution of Cr by Fe in MIL-101 framework and its application as a novel heterogeneous photo-Fenton catalyst for reactive dye degradation, RSC Adv. 4 (78) (2014) 41185–41194.
[82] L. Xie, D. Liu, H. Huang, Q. Yang, C. Zhong, Efficient capture of nitrobenzene from waste water using metal–organic frameworks, Chem. Eng. J. 246 (2014) 142–149.
[83] S. Liu, J. Wang, W. Huang, X. Tan, H. Dong, B.A. Goodman, H. Du, F. Lei, K. Diao, Adsorption of phenolic compounds from water by a novel ethylenediamine rosin-based resin: Interaction models and adsorption mechanisms, Chemosphere 214 (2019) 821–829.
[84] Y. Gao, K. Liu, R. Kang, J. Xia, G. Yu, S. Deng, A comparative study of rigid and flexible MOFs for the adsorption of pharmaceuticals Kinetics, isotherms and mechanisms, J. Hazard. Mater. 359 (2018) 248–257.
[85] F. Qin, S. Jia, Y. Liu, H. Li, S. Wu, Adsorptive removal of bisphenol A from aqueous solution using metal-organic frameworks, Desalin. Water Treat. 54 (1) (2015) 93–102.
[86] P.E. Young, H. Zubair, K.N. Abedin, J.S. Hwa, Adsorptive removal of bisphenol-A from water with a metal-organic framework, a porous chromium-benzenedicarboxylate, J. Nanosci. Nanotechnol. 13 (4) (2013) 2789–2794.
[87] C.A. Hunter, J. Singh, J.M. Thornton, π-π interactions: the geometry and energetics of phenylalanine-phenylalanine interactions in proteins, J. Mol. Biol. 218 (4) (1991) 837–846.
[88] A.M. Puziy, O.I. Poddubnaya, R.P. Socha, J. Gurgul, M. Wisniewski, XPS and NMR studies of phosphoric acid activated carbons, Carbon 46 (15) (2008) 2113–2123.
[89] J.V. Bothe, P.W. Brown, Arsenic immobilization by calcium arsenate formation, Environ. Sci. Technol. 33 (21) (1999) 3806–3811.